UC Riverside

UC Riverside Previously Published Works

Title

Comparing accuracy and reproducibility of sequential and Hadamard-encoded multidelay pseudocontinuous arterial spin labeling for measuring cerebral blood flow and arterial transit time in healthy subjects: A simulation and in vivo study

Permalink

https://escholarship.org/uc/item/9g10h380

Journal

Journal of Magnetic Resonance Imaging, 47(4)

ISSN

1053-1807

Authors

Guo, Jia
Holdsworth, Samantha J
Fan, Audrey P
et al.

Publication Date

2018-04-01

DOI

10.1002/jmri.25834

Peer reviewed

eScholarship.org Powered by the California Digital Library
University of California

Author Manuscript

Author Manuscript

Author Manuscript

Author Manuscript

HHS Public Access

Author manuscript

J Magn Reson Imaging. Author manuscript; available in PMC 2019 April 01.

Published in final edited form as:

J Magn Reson Imaging. 2018 April ; 47(4): 1119–1132. doi:10.1002/jmri.25834.

Comparing accuracy and reproducibility of sequential and Hadamard-encoded multi-delay PCASL for measuring CBF and ATT in healthy subjects – a simulation and in vivo study

Jia Guo, PhD[1,*], **Samantha J. Holdsworth, PhD**[1], **Audrey P. Fan, PhD**[1], **Marc R. Lebel, PhD**[2], **Zungho Zun, PhD**[3,4], **Ajit Shankaranarayanan, PhD**[5], and **Greg Zaharchuk, PhD, MD**[1]

[1]Department of Radiology, Stanford University, Stanford, CA, United States

[2]GE Healthcare, Calgary, Canada

[3]Diagnostic Imaging and Radiology, Children's National Medical Center

[4]Department of Pediatrics, George Washington University, Washington, DC, United States

[5]GE Healthcare, Menlo Park, CA, United States

Abstract

Background—Multi-delay arterial spin labeling (ASL) can measure both cerebral blood flow (CBF) and arterial transit time (ATT).

Purpose—To compare performance of sequential and Hadamard-encoded pseudo-continuous ASL (PCASL).

Study type—Cohort.

Subject—Monte Carlo simulations and in vivo experiments in 10 healthy subjects.

Field strength and sequence—5-delay sequential (5-del. Seq.), 7-delay Hadamard-encoded (7-del. Had.), and a single-delay (1-del.) PCASL, without and with vascular crushing at 3.0 T.

Assessment—The errors and variations of CBF and ATT from simulations and the CBF and ATT estimates and variations in gray matter (GM) with different ATT ranges were compared.

Statistical tests—Pairwise t-tests with Bonferroni correction.

Results—The simulations and in vivo experiments showed that 1-del. PCASL underestimated GM CBF due to insufficient post-labeling delay (PLD) (37.2 ± 8.1 vs. 47.3 ± 8.5 and 47.3 ± 9.0 ml/100g/min, $p \leq 6.5 \times 10^{-6}$), while 5-del. Seq. and 7-del. Had. yielded comparable GM CBF ($p \geq 0.49$). 5-del. Seq. was more reproducible for CBF ($p = 4.7 \times 10^{-4}$), while 7-del. Had. was more reproducible for ATT ($p = 0.033$). 5-del. Seq. was more prone to intravascular artifacts and yielded lower GM ATTs compared to 7-del. Had. without crushing (1.13 ± 0.18 vs. 1.23 ± 0.13 s, $p = 2.3 \times 10^{-3}$), but they gave comparable ATTs with crushing ($p = 0.12$). ATTs measured with crushing were longer than those without crushing ($p \leq 6.7 \times 10^{-4}$), but CBF was not affected ($p \geq 0.16$).

[*]**Correspondence to:** Jia Guo, PhD, The Richard M. Lucas Center for Imaging, 1201 Welch Rd, Stanford University, Stanford, CA 94305, guojia@stanford.edu.

Author Manuscript Author Manuscript Author Manuscript Author Manuscript

The theoretical signal-to-noise ratio (SNR) gain through Hadamard encoding was confirmed experimentally.

Data conclusion—For 1-del., a PLD of 1.8 s is recommended for healthy subjects. With current parameters, 5-del. Seq. was more reproducible for CBF, and 7-del. Had. for ATT. Vascular crushing may help reduce variations in multi-delay experiments without compromising tissue CBF or ATT measurements.

Keywords

Arterial spin labeling; Pseudo-continuous ASL; Multi-delay ASL; Reproducibility; Arterial transit time; Cerebral blood flow

Introduction

Arterial spin labeling (ASL) is an MRI method to measure cerebral blood flow (CBF) non-invasively (1–3). It uses radiofrequency (RF) and gradient pulses to label the spins in arterial blood. In conventional ASL methods, including pulsed ASL (PASL) (4–7), continuous (or pseudo-continuous) ASL (CASL/PCASL) (1,3,8), a physical gap is prescribed between the labeling and imaging sites to reduce the interference of the labeling pulses to the imaging region. This gap requires some time, called arterial transit time (ATT), for the labeled blood to enter the imaging voxels and reach the capillary bed. Just like CBF (9–11), ATT may contain valuable and complementary hemodynamic information (12–14). ATT can be measured by collecting and fitting ASL signals at different post-labeling times (PLDs) (14,15) to a dynamic ASL model such as described in (16), or by measuring ASL signals with and without vascular crushing (17). According to a recent consensus in the ASL community (18), PCASL is recommended for clinical use for its high signal-to-noise ratio (SNR). ATT estimation using PCASL is typically conducted by multi-delay measurements, where the ASL signal at different PLDs are collected in a sequential manner.

Recently, time-encoded multi-delay acquisition (19), e.g. using a Hadamard matrix to encode multiple sub-boluses, has demonstrated SNR and temporal efficiency improvement compared to sequential acquisition in rats (20) (with improved ATT but degraded CBF estimation) and human subjects (21). The study in (21) used the same short labeling durations (LDs) in sequential and Hadamard-encoded labeling to demonstrate the SNR gain with Hadamard encoding. However, using short LDs is not optimal for sequential acquisitions, as it substantially limits the SNR. In a more recent study (22), sequential and Hadamard-encoded labeling were compared through simulation and in vivo experiments with a set of better matched labeling parameters. However, the study was limited by suboptimal imaging parameters (e.g., 2D acquisition without background suppression (BS)); the accuracy was not thoroughly compared; and the reproducibility was not examined. Therefore, it is not clear how the two multi-delay labeling strategies compare in practical settings with more advanced implementations of ASL, in terms of SNR, reproducibility and estimation accuracy. The main goal of this study was to compare the performance of CBF and ATT measurements using sequential and Hadamard-encoded multi-delay PCASL, through Monte Carlo simulations and in vivo experiments in healthy human subjects, with matched labeling parameters and similar, clinically-relevant total scan durations.

Author Manuscript Author Manuscript Author Manuscript Author Manuscript

Materials and Methods

Monte Carlo simulations

The simulations were carried out in MATLAB 2015b (The Mathworks, Natick, USA). Twenty thousand pairs of CBF and ATT, evenly distributed within [30–90] ml/100 g/min and [0.4–2.0] s, respectively, were used as the ground truth. The following PCASL signal model, derived from the general kinetic model of Buxton (16,23) was used to generate the ASL signal at the i-th PLD (PLD_i):

$$S_{ASL,i}=2\cdot M_{t,0}\cdot CBF\cdot\alpha\cdot T_{1t}\cdot e^{-\frac{ATT}{T_{1a}}}\cdot\left(e^{\frac{-\max(PLD_i-ATT,0)}{T_{1t}}}-e^{\frac{-\max(PLD_i+LD_i-ATT,0)}{T_{1t}}}\right)/\lambda \quad \text{Eq. 1}$$

where $M_{t,0}$ is fully relaxed brain tissue magnetization in equilibrium, α is the labeling efficiency, T_{1t} and T_{1a} are the T_1 of tissue and arterial blood, respectively, LD_i is the i-th labeling duration (LD), and λ is the tissue-to-blood partition coefficient of water. It is assumed that the spins rapidly transfer from blood to tissue once they reach the tissue (23), due to a much larger water pool in the tissue than in the capillary bed. In the simulation, $M_{t,0}$, α and λ were set to 1 (as there are only scaling factors), while T_{1a} and T_{1t} were set to 1.65 s (18,24) and 1.5 s (25), respectively.

Three PCASL methods (two multi-delay and one single-delay) were simulated with the following parameters: 1) 5-delay sequential-encoded labeling (5-del. Seq.) with $LD_{1–5}$ = 2000 ms, $PLD_{1–5}$ = 300, 1025, 1750, 2475 and 3200 ms, 1 average; 2) 7-delay Hadamard-encoded labeling (7-del. Had.) with effective $LD_{1–7}$ = 700 ms, $PLD_{1–7}$ = 300, 1000, 1700, 2400, 3100, 3800, 4500 ms, 1 average; 3) standard single-delay labeling (1-del.) with LD/PLD = 1450/1525 ms, 6 averages. The 1-del. ASL was included for reference. To be consistent with the in vivo experiments, the implementation of 7-del. Had also included an extra encoding step with all the sub-boluses under control condition, which only reduced the SNR efficiency by about 2.6% compared to the original Hadamard scheme. A recovery time of 2 s and 4-shot imaging were assumed. We chose these labeling parameters so the labeling and total scan time were roughly matched, and similar to those used in the in vivo experiments (see below).

Zero-mean Gaussian noise was added in each acquisition, that is, in each label and control step in 1-del. or 5-del. Seq. methods, or each encoding step in 7-del. Had. method. The noise was applied with 125 levels of relative SNR (rSNR, from 0.2 to 25 with a step size of 0.2), with the standard deviation (SD) of the noise calculated with respect to the theoretical ASL signal from a pair of label and control acquisition with LD/PLD/ATT = 1000/2000/0 ms. In other words, at a given rSNR level, the same amount of noise was added to each image acquisition in the ASL experiments, whether or not Hadamard encoding was used.

For the multi-delay methods, a signal-weighted delay approach (26) was used to estimate the ATTs. ATT-corrected CBF values were calculated through a weighted sum of the ASL signals at different PLDs, with the weights being normalized by the theoretical ASL signals at those PLDs, according to Eq. 1. For the single-delay method, CBF values were calculated

Author Manuscript Author Manuscript Author Manuscript Author Manuscript

based on Eq. 1, with ATT = 0 ms and $T_{1t} = T_{1a} = 1.65$ s given that the ATT information was not available in the single-delay measurements.

To examine the reproducibility of these methods, the simulation was repeated twice on these twenty thousand CBF/ATT instances to simulate the test and retest conditions. The difference of CBF and ATT estimates between the test and retest were normalized to the corresponding true values. The SD of the difference was calculated and used as the metric of reproducibility (21), i.e., lower the SD indicates higher reproducibility. The difference between the true values and the averaged estimates of CBF and ATT from the repeated simulations were calculated and normalized to the true values. The mean of the normalized difference was then calculated and used as the estimation error of these methods. The test and retest simulations were repeated 100 times (i.e. 4 million instances of CBF and/or ATT estimation in total) and the mean values of the normalized SD and the estimation error were reported at each rSNR level. To explore if there is any performance dependence on ATT values, the CBF and ATT combinations were grouped into low (0.4 – 1.2 s) and high (1.2 – 2.0 s) ATT groups and the above analysis was performed. The performance dependence on CBF was not examined because the SNR scales linearly with CBF values, so the performance can be directly inferred from the performance with respect to SNR levels.

In vivo experiments

Ten normal healthy subjects (3 Females, 25 – 63 y.o., 37.2 ± 11.4 y.o.,) were studied in a 3.0T GE scanner (MR750, GE Healthcare, Waukesha WI) with an 8-channel receive-only head coil. The study complied with regulations of the local Institutional Review Board (Administrative Panels for the Protection of Human Subjects) and written consent was obtained from each subject.

The PCASL images were acquired with a 4-shot 3D fast spin echo stack of spiral readout, 512 points per arm, field of view (FOV) = 240 × 240 mm^2, in-plane resolution = 5.77 × 5.77 mm^2, reconstructed to 1.875 × 1.875 mm^2, 28 slices with 5 mm thickness. The labeling parameters were chosen to closely match to those used in the simulations. Similar labeling times between the two multi-delay methods and similar total scan times for the three methods were achieved:

1. Sequential-encoded labeling (5-del. Seq.): repetition time (TR)/echo time (TE) = 6566/10.7 ms, $LD_{1–5}$ = 2000 ms, $PLD_{1–5}$ = 300, 1025, 1750, 2475 and 3200 ms, number of averages = 1, total scan time = 4 min 50 s;
2. Hadamard-encoded labeling (7-del. Had.): TR/TE = 6566/10.7 ms, $LD_{1–7}$ = 700 ms, effective $PLD_{1–7}$ = 300, 1000, 1700, 2400, 3100, 3800, 4500 ms, number of averages = 1, total scan time = 4 min 25 s;
3. For reference, conventional single-delay PCASL labeling (1-del.) data were also collected with: TR/TE = 5466/10.7 ms, LD/PLD = 1450/1525 ms, number of averages = 6, total scan time = 4 min 44 s.

The total scan times also included acquisition of a saturation recovery reference image, with a saturation time of 2000 ms, for CBF quantification. Saturation pulses before labeling and BS inversion pulses (four in multi-delay and five in single-delay, respectively) were applied

Author Manuscript Author Manuscript Author Manuscript Author Manuscript

to null tissues with T_1 ranging from 800 ms to 3000 ms for improved SNR. The BS timings for 5-del. Seq. and 7-del. Had. were identical. To study the effects of vascular crushing (17,27) on CBF and ATT estimation, the scans were repeated with and without vascular crushing using a 4-segment B_1-insensitive rotation (BIR-4) pulse module (28) with a cutoff velocity (v_{cut}) of 2 cm/s in the S/I direction, i.e., equivalent to VENC = 4 cm/s as recommended in (18), and an effective TE of 7.5 ms. The scans followed the order of 1-del., 5-del. Seq. and 7-del. Had., repeated after about 15 minutes, to study the test-retest reproducibility of these methods. T_1-weighted anatomical images were collected with an inversion-recovery prepared 3D fast SPGR sequence (TR/TE = 9.5/3.8 ms, inversion time = 400 ms, spatial resolution = $0.94 \times 0.94 \times 1$ mm^3).

The CBF and ATT maps were reconstructed following the same processing described in the simulation section. For CBF quantification, a labeling efficiency of 0.85 (8) and an average partition coefficient of 0.9 ml/g (29) were assumed. The fully relaxed magnetization of brain tissue, $M_{t,0}$, was calculated from the reference images. In the reference image acquisition, the same vascular crushing condition as in the ASL acquisition was applied, so that the signal loss due to vascular crushing should be canceled out. The signal loss due to BS was also accounted for with an assumed efficiency of 0.75 (30).

T_1-weighted images were first brain-extracted using the BET routine in the FMRIB Software Library tool (FSL) (32), and then normalized into the Montreal Neurological Institute (MNI) brain template space (31) using NiftyReg software, with a linear registration step followed by a non-linear step. Whole brain gray matter (GM) regions of interest (ROIs) were obtained for each subject on the normalized T_1-weighted images using the FAST routine in FSL for subsequent analysis, with a default partial volume probability threshold of 0.5. For CBF and ATT maps from each subject, a linear transformation matrix was calculated by registering the averaged ASL images in each scan to the anatomical images, and was combined with those generated in the anatomical-to-MNI step to normalize CBF and ATT maps into the MNI space. All the registration results were visually inspected to ensure no obvious mis-registration occurred. The CBF and ATT differences between the test and retest runs were calculated for each PCASL sequence and crushing condition in each voxel, and were then normalized to the mean values of the two runs. The mean and the SD of the normalized difference were calculated in the GM ROI. The SD was used as a measure of reproducibility as in the simulations. This processing is demonstrated in Figure 1. Averaged CBF and ATT values in GM ROI were first calculated across the test and retest runs in each subject, followed by calculation of the mean and SDs across subjects. The SNR in each ASL scan was measured in an ROI containing the middle 16 slices of the original ASL difference images after correction for the receive-coil sensitivity. The original ASL difference images were used to minimize the influence of post-processing steps on the noise statistics, especially outside the brain. Mean ASL signals at each PLD were measured in the GM masks generated (with a threshold of 0.7×90^{th} percentile of the ASL signals) from the mean ASL images, which were obtained by a simple averaging across all PLDs. SD of the noise was measured in a hand-drawn ROI outside of the brain at a similar location across subjects that avoided any obvious artifact and spanned the 16 slices (≥ 7520 voxels in total). The SNR was then calculated as S_{ASL}/SD_{noise} and averaged between the repeated scans. Averaged SNR values across subjects are reported. For the single-delay measurement, the

Author Manuscript Author Manuscript Author Manuscript Author Manuscript

measured SNR was divided by $\sqrt{6}$ (i.e., 6 averages) to give a SNR metric that can be directly compared to the other two multi-delay measurements. To better compare between the simulations and the in vivo measurements, the SNRs were also converted to the rSNR levels – divided by the ratio of expected theoretical ASL signal in the actual measurement and the reference ASL signal described in the simulation section. For the 5-del. Seq. data, only the rSNR level at PLD = 1.75 s was calculated, as this is close to the PLD used in 1-del. measurements. Note that the rSNR level for 7-del. Had. data was not calculated due to the Hadamard-encoding process; instead, rSNR (i.e., noise) levels similar to those measured in 5-del. Seq. scans were assumed, given the fact that the BS timings were matched between the two sequences, therefore similar levels of BS and physiological noise were expected.

Similar to that in the simulation, the above analysis was also carried out in the GM voxels with low (ATT ≤ 1.2 s) and high (ATT > 1.2 s) ATTs separately. To minimize potential bias in ROI selection, the ROIs were derived from mean ATT maps averaged between those acquired with 5-del. Seq. and 7-del. Had. For the analysis on the average measurements and test-retest variations, the ATT specific ROIs were generated from the ATT maps in the MNI space; while for the SNR analysis, they were generated from those in the native space.

Statistical analysis

Pairwise t-tests were performed on the average CBF and ATT measurements and the normalized difference SD, between sequences, crushing conditions and between the GM regions with low and high ATT values. To reduce the chance to make a type I error, a conservative Bonferroni correction was applied on a significance detection threshold of 0.05 for multiple comparisons.

Results

Simulations

The mean normalized errors in CBF and ATT estimation are shown in Figures 2a and b. 1-del. sequence showed relatively constant 7.5% and 18.3% underestimation at low ATT and high ATT values, respectively, and on average 12.3% underestimation of CBF across rSNRs. The estimation errors of 5-del. Seq. and 7-del. Had. sequences rapidly decreased when rSNR > 2.2 and 2.4, respectively. When rSNR > 3.0, both multi-delay sequences yielded mean normalized errors less than 2.0% on average. Compared to 5-del. Seq., 7-del. Had. showed smaller errors in CBF estimation at very low SNR levels (rSNR < 1.8), but had slightly higher errors when rSNR > 1.8 (Figure 2a), especially with ATT > 1.2 s. Overall, 5-del. Seq. yielded more consistent and accurate CBF estimation across these two ATT ranges. For ATT estimation, 7-del. Had. produced less biased (smaller estimation error) estimates of ATT than 5-del. Seq. overall. The mean errors of these two sequences were low (< 1%) when SNR was high (rSNR > 2.0). Interestingly, both multi-delay sequences tended to overestimate low ATT values (≤ 1.2 s) and underestimate high ATT values (> 1.2 s) when the SNR was low (rSNR < 3.0). When SNR improved, 5-del. Seq. showed persistent negative biases in ATT estimation in both ATT ranges; while 7-del. Had. showed mixed but overall smaller biases (Figure 2b).

Author Manuscript Author Manuscript Author Manuscript Author Manuscript

The mean values of the normalized SD in CBF and ATT between the repeated measurements are shown in Figures 2c and d. For the three PCASL sequences simulated, the normalized SD for CBF for all ATT dropped quickly once the rSNR was sufficiently high, with the knee points (33) being 2.2, 1.8 and 2.0 for 1-del., 5-del. Seq. and 7-del. Had. sequences, respectively. Due to the noise reduction from signal averaging, the 1-del. sequence showed the lowest normalized SDs, i.e., the highest reproducibility, in CBF measurements, consistent across different ATT ranges. Compared to 5-del. Seq., 7-del. Had. had lower variations in CBF measurement with rSNR < 1.3, and higher variations with rSNR > 1.3, and this pattern was consistent across different ATT ranges (Figure 2c). For ATT estimation, 7-del. Had. showed overall less dependence on the ATT ranges and was more reproducible at estimating high ATT values compared to 5-del. Seq. (Figure 2d), but not as reproducible at estimating low ATT values. Across all ATT values, 7-del. Had. was more reproducible overall.

In vivo experiments

The raw ASL signals from a representative subject at different PLDs are shown in Figure 3. The mean CBF and ATT maps and averaged estimates in GM ROI across subjects are shown in Figures 4 and 5. The averaged values are also summarized in Table 1, top section.

Compared to the two multi-delay methods, 1-del. yielded lower CBF values globally, as well as lower CBF estimates in watershed and posterior cortical regions where long ATTs were expected compared to other regions in the brain, e.g., the 4^{th} and 5^{th} slices shown in Figures 4a and b. Vascular crushing led to a small but noticeable decrease in CBF measured by 1-del. PCASL, but did not affect CBF quantification for the multi-delay PCASL sequences. Quantitatively, the mean CBF values in all GM ROIs were 38.4 ± 7.4 and 37.2 ± 8.1 ml/100 g/min measured by 1-del. PCASL, 47.5 ± 7.1 and 47.3 ± 8.5 ml/100 g/min by 5-del. Seq. PCASL, and 46.8 ± 8.1 and 47.3 ± 9.0 ml/100 g/min by 7-del. Had. PCASL, without and with vascular crushing, respectively. Looking at CBF measurements with vascular crushing, 1-del. underestimated CBF by 12.9% ($P = 7.2 \times 10^{-6}$) and 13.1% ($P = 1.3 \times 10^{-4}$) in low ATT GM regions compared with 5-del. Seq. 7-del. Had., respectively; and underestimated CBF by 25.5% ($P = 7.2 \times 10^{-7}$) and 25.8% with crushing ($P = 3.0 \times 10^{-7}$) in high ATT regions. The underestimation was consistent with the simulation results (7.5% and 18.3%, Figure 2a). There was no significant difference detected between the two multi-delay PCASL methods ($P > 0.19$). No significant difference of GM CBF estimates between different crushing conditions was detected with each PCASL method except that 5-del. Seq. measured lower CBF in low ATT regions with crushing ($P = 0.031$, Table 3), indicating stronger intravascular effect than other sequences. Both multi-delay methods detected higher CBF in high ATT regions compared to low ATT regions with crushing (5.7% and 5.9% for 5-del. Seq. and 7-del. Had., $P = 9.9 \times 10^{-3}$ and 5.6×10^{-3}, respectively).

For ATT estimation, both multi-delay methods detected expected longer ATTs in watershed regions compared to other regions in the brain (Figures 4c and d), as well as longer ATTs in white matter (WM) than in GM. In general, estimated ATTs appeared longer as the slice location moved higher, reflecting the longer transit of blood to reach higher slices. Overall, measured ATTs were longer with vascular crushing than without. 5-del. Seq. gave lower

Author Manuscript Author Manuscript Author Manuscript Author Manuscript

ATTs in voxels where large arteries reside (e.g., the 2nd and 3rd slices in Figure 4c, top row indicated by white arrows), reflecting some strong intravascular signal contribution; this effect was largely mitigated yet still noticeable with vascular crushing (Figure 4d, top row). In contrast, this intravascular artifact was not observed with 7-del. Had. labeling, i.e., the ATT maps were very similar with and without vascular crushing, with only slightly longer ATTs observed with crushing. Quantitatively, the mean ATT in GM measured by 5-del. Seq. was significantly shorter than that by 7-del. Had. without crushing, i.e., 0.84 ± 0.071 s vs. 0.92 ± 0.041 s, $P = 3.9 \times 10^{-6}$ in low ATT ROIs, 1.31 ± 0.13 s vs. 1.48 ± 0.14 s, $P = 1.0 \times 10^{-4}$ in high ATT ROIs, and 1.13 ± 0.18 s vs. 1.27 ± 0.20 s, $P = 2.3 \times 10^{-3}$ in all ATT ROIs. With vascular crushing, 5-del. Seq. still gave slightly shorter ATT in GM with crushing compared to 7-del. Had., i.e., 1.05 ± 0.044 s vs. 1.09 ± 0.049 s in low ATT ROIs, 1.34 ± 0.097 s vs. 1.47 ± 0.082 s in high ATT ROIs and 1.23 ± 0.13 s vs. 1.32 ± 0.13 s in all ATT ROIs, but no significance was detected ($P \geq 0.12$). Vascular crushing significantly increased the mean ATTs estimated in GM with both multi-delay methods ($P \leq 0.018$) in all the ATT ranges examined.

The averaged normalized variation of CBF and ATT in GM between the repeated scans were shown in Figure 6 and summarized in Table 1, right section.

For CBF measurements, 1-del. was the most reproducible (*P*-values shown in Table 2, right section), both without and with crushing, mainly due to more signal averaging and the fact that only one parameter was estimated. Without vascular crushing, 5-del. Seq. and 7-del. Had. were comparably reproducible in CBF measurement in all ATT ranges; however, with vascular crushing, 5-del. Seq. was more reproducible than 7-del. Had. ($P \leq 7.7 \times 10^{-4}$). All three sequences showed similar reproducibility with and without vascular crushing ($P \geq 0.062$ Table 3, bottom left section).

For ATT measurement, 7-del. Had. was more reproducible than 5-del. Seq. in all ATT ranges without crushing ($P \leq 9.0 \times 10^{-5}$). With crushing, 7-del. Had. had higher reproducibility in low ATT ROI ($P = 3.3 \times 10^{-4}$) or when all GM voxels were examined ($P = 0.033$) but had similar reproducibility in high ATT ROI ($P = 0.52$), compared to 5-del. Seq. Note that vascular crushing significantly improved the reproducibility of 5-del. Seq. in ATT measurement in high ATT ROI ($P = 1.3 \times 10^{-3}$) and when all ATT ROIs were examined ($P = 8.1 \times 10^{-3}$), but did not show a big effect in low ATT ROI ($P = 0.26$). For 7-del. Had., crushing did not affect the reproducibility of ATT measurement in all ATT ranges ($P \geq 0.45$).

The measured SNR of ASL signals are shown in Table 4. Overall, the SNRs with vascular crushing were lower than that without crushing, due to signal attenuation from the crushing pulses, and decreased contribution of the intravascular signals at early PLDs. In the following, we focused on the SNR measurements with vascular crushing, which should be less biased and reflect the measurement in tissue perfusion. For 5-del. Seq., the SNR started high due to long LDs, peaked at PLD_2 and then decreased as T_1 relaxation dominated; while for 7-del. Had., the SNR increased from zero at PLD_1 when almost no labeled spins reached the tissue, peaked at PLD_3 and then decreased. Both multi-delay methods had higher SNRs in low ATT ROIs than in high ATT ROIs before PLD_3 ($P \leq 8.6 \times 10^{-3}$), also confirming the early arrival of ASL signal in low ATT ROIs; when the PLD was sufficiently long (after

Author Manuscript Author Manuscript Author Manuscript Author Manuscript

PLD_2 for 5-del. Seq. and PLD_3 for 7-del. Had.), the SNRs were lower in low ATT ROIs than in high ATT ROIs ($P \leq 1.9 \times 10^{-4}$), possibly due to higher CBF (see Table 1) and/or less T_1 decay of the ASL signal in high ATT ROIs, since the labeled spins in such regions will have spent proportionally more time in the arterial blood compared with the tissue, where the T_1 is shorter. At comparable PLDs, the SNRs in GM ROIs with both low and high ATT were 8.73 ± 2.12, 9.72 ± 2.13, and 9.97 ± 2.71 for 1-del. at PLD = 1525 ms, 5-del. Seq. at PLD_3 = 1700 ms and 7-del. Had. at PLD_3 = 1750 ms, respectively. With similar LDs, PLDs and BS levels, the SNRs for 1-del. and 5-del. Seq. were comparable, as expected. For 7-del. Had., though it used an over 2-fold shorter LD compared with 5-del. Seq. (700 vs. 2000 ms), the noise level was only half $(\sqrt{2/(N+1)}, \mathrm{N}=7)$ due to the Hadamard encoding scheme (21), resulting in a comparable SNR. Using a reference ASL signal described in the simulation section, the rSNR levels were 4.61 ± 1.12 for single-delay and 5.02 ± 1.10 for multi-delay measurements in GM ROIs. At these rSNR levels, the measured normalized variations of CBF and ATT measurements were consistent with those predicted by the simulations (Table 1 right section and Figures 2c and d). An interesting finding is that the measured normalized variations of ATT by 5-del. Seq. followed the trend predicted in the simulation; however, the expected lower variation compared with 7-del. Had. in high ATT ROI was not observed in vivo.

Discussion

In this study, we compared the quantification and short-term reproducibility of two multi-delay PCASL sequences in simulations and healthy subjects. The labeling parameters were closely matched for fair comparisons, given matched total scan times that were clinically-relevant.

Without vascular crushing, ATT measures the time labeled spins arrive in the imaging voxels, not necessarily in microvasculature; while with vascular crushing, ATT reflects the time at which labeled spins reach the microvasculature (17,18). Therefore, the assumption of Eq. 1 that the spins exchange immediately from arterial to tissue compartment upon arrival to the imaging voxels should be more valid with vascular crushing. In turn, Eq. 1 should give more accurate estimation of the time labeled spins spend in each compartment, and thus a more accurate estimation of CBF. Following the discussion above, the simulations based on Eq. 1 should fit the in vivo data acquired with vascular crushing the best. Indeed, the reproducibility of CBF and ATT estimation from in vivo measurements matched closely to the predicted values from the simulations at the measured SNR levels. A similar trend on CBF and ATT estimation errors using sequential- and Hadamard-encoded labeling was also observed from simulation in (20). By analyzing the results in different ATT ranges, we could observe the performance difference between these labeling methods with respect to different ATT ranges. These results validated our approach of studying labeling methods through the modeling and simulation, which should provide useful theoretical guidelines for conducting ASL experiments in other populations where the ATT ranges may significantly differ from the healthy population, such as elderly or diseased populations.

Author Manuscript Author Manuscript Author Manuscript Author Manuscript

Intravascular signals affected 5-del. Seq. more than 7-del. Had., especially in regions where large arteries reside. Even after application of vascular crushing, the contribution from the intravascular signal and its effect on ATT estimation was still visible using 5-del. Seq. This was likely because the total labeling duration was kept identical in this study, the long LDs used in 5-del. Seq. resulted in smaller maximal PLDs that were available, compared to 7-del. Had. As discussed in (26), a long LD may introduce some sensitivity to tissue T_1 in ATT estimation. In addition, a long continuous LD is more likely to accumulate strong intravascular ASL signals at short PLDs, compared to shorter sub-boluses under different label/control conditions in encoded methods, resulting in stronger weighting towards measurements at these earlier arrival times. The observation that crushing significantly reduced variation in ATT estimation in high ATT ROIs in 5-del. Seq. suggested that long LDs might have also increased the ASL signal variation (potentially from the intravascular signal) at long PLDs due to the dispersion of the labeled bolus (34,35). These effects in principle can be mitigated by vascular crushing and was confirmed by improved test-retest reproducibility in ATT estimation. As discussed above, short LDs may give more accurate and robust ATT estimation than long LDs; however, short LDs limit the SNR of ASL signals and the robustness of the measurements. Therefore, intermediate LDs may be considered as a tradeoff. From another perspective, the intravascular signal can be modeled (36) to improve the accuracy of ATT estimation in multi-delay ASL.

CBF underestimation using 1-del. PCASL was observed in both simulations and in vivo experiments. The reason was twofold. First, the PLD of 1.525 s was insufficient compared to the ATT ranges encountered, e.g., 0.4 – 2.0 s in simulations and 0.59 – 1.87 s (the widest range, calculated with mean ± 3 standard error of the mean) in healthy subjects. To reduce underestimation from this cause, a longer PLD should be used. In this study, the voxels with ATT > 1.8 s were less than 1.1% in GM, confirming the validity of the recommended PLD of 1.8 s to be used with PCASL in healthy subjects < 70 y. o. (18). Second, because the ATT information was typically not available for 1-del. measurement, only the T_1 of arterial blood was used in the quantification, so the faster ASL signal decay in the tissue due to a shorter T_1 was not accounted for. To mitigate this effect, in addition to using a correct tissue T_1, a population-averaged value of ATT may be assumed in quantification. This way, while the CBF in regions with shorter ATT would be overestimated, the overall errors should be reduced.

While recognizing the importance of correcting for ATT and relaxation in tissue as discussed above, CBF quantification is relatively robust to ATT estimation errors, given that the ATT is within the PLD range. For example, compared to 7-del. Had. without crushing, 5-del. Seq. underestimated ATT by about 8.1% in GM on average, but it only overestimated CBF by about 1.5%.

In addition to reducing the intravascular signal, vascular crushing slightly reduced the ASL signal due to the T_2 relaxation during the crushing pulses. Because the same vascular crushing pulses were also used in the reference scan, a similar T_2 relaxation was expected and should cancel out in quantification, resulting in accurate CBF quantification in multi-delay acquisitions. As confirmation, measured CBF values were almost identical with and without vascular crushing.

Author Manuscript Author Manuscript Author Manuscript Author Manuscript

SNR improvement from Hadamard encoding was observed compared to sequential encoding, with similar LD and PLD parameters, consistent with the theory and findings in literature (19–21). This SNR improvement compensated for the reduction from using short LDs in 7-del. Had., yielding comparable SNRs with 5-del. Seq. This property makes Hadamard-encoding appealing in ASL experiments, because shorter LDs can be traded for a bigger PLD covering range without sacrificing SNR, given a fixed total labeling time. However, there are some limiting aspects of Hadamard encoding. First, sensitivity to motion is more concerning in time-encoded acquisitions. For example, if one of encoded acquisition is corrupted by motion, all the decoded measurements dependent on the data from this step would be affected. Prospective motion correction methods, like PROMO (37,38), and re-ordering schemes, like Walsh-ordered encoding (39), can be adopted to reduce the motion sensitivity. Second, though Hadamard encoding has an optimal SNR efficiency of 1, the number of Hadamard encoding steps is not freely adjustable, e.g., to encode multiple sub-boluses, the number of encoding steps (i.e., the order of Hadamard matrices) has to be a multiple of 4. Given a limited total LD, it may be worth utilizing some sub-optimal encoding schemes that can still provide some SNR advantage while allowing some freedom on the number of encoding steps to collect.

In this study, we conducted the measurement and comparison in GM. Though the CBF and ATT values were also calculated in WM, these values were likely to be underestimated for the following reasons. In this study, T_{1t} of GM was used for the whole brain, including WM which typically has a shorter T_{1t}, this would have led to an underestimation of ATT. Consequently, an underestimated ATT would lead to an overestimation of CBF. However, as some simple calculations can show, this overestimation was smaller than the underestimation caused by the use of T_{1t} of GM instead of WM, resulting in general underestimation of CBF in WM. Similarly, it was also likely that CBF and ATT were underestimated in GM regions where the tissue T_1 is shorter. A T_1 map of the tissue, such as acquired in (26), should help improve the quantification accuracy in these regions.

There were limitations in this study. First, the labeling parameters were chosen based on our experience for a practical and fair comparison. Though we spent effort matching the timings for each labeling method, further optimization may be needed. In fact, optimizing the labeling parameters for different applications/populations in multi-delay ASL is an active research topic, e.g., in (22,40), which was not covered in the current study. In addition, though single-delay ASL was included mainly for reference purpose, the labeling parameters in 1-del. can also be optimized for targeting specific ATT ranges. Second, the findings were limited to the labeling parameters used in this study. Nevertheless, the current study explored and compared the aspects that were not covered previously, and should help guide future research on optimizing and comparing these ASL methods. Third, the interval between the test/retest scans were kept short (~15 minutes) to study the short-term reproducibility of the labeling methods, but the order of the scanning was not randomized. Subjects were only asked to “relax” during the scans, but possible physiological/vigilance status changes might have occurred throughout the session and introduced additional variations between the scans. Fourth, though we found good consistency between the results of the simulation and the in vivo experiments in 10 healthy subjects, a larger number should be included for a better in vivo validation. Last, though all the data passed human inspection

Author Manuscript Author Manuscript Author Manuscript Author Manuscript

for motion corruption and were co-registered to the individual anatomical images, no additional motion correction was applied.

In conclusion, we conducted a reproducibility comparison between standard 1-del., 5-del. Seq. and 7-del. Had. PCASL labeling methods in healthy subjects under similar total scan times, focusing on the multi-delay methods. Standard 1-del. method should give most reproducible results, but can underestimate CBF if PLD is not sufficiently long. With current implementation, 5-del. Seq. showed higher reproducibility in CBF measurement, while 7-del. Had. was more reproducible in ATT measurement, consistent with the simulation results. The SNR gain by Hadamard encoding was confirmed. With some optimization, Hadamard encoded labeling strategy is likely to provide robust measurements of both CBF and ATT in a time-efficient way. Vascular crushing should help reduce variations in multi-delay ASL experiments without compromising the accuracy of CBF estimation, while giving ATTs in tissue that may be clinically meaningful.

Acknowledgments

A.P. Fan is funded by Stanford Neuroscience Institute Interdisciplinary Scholar Award.

Grant Support:

NIH 5R01NS066506, NCRR 5P41RR09784, and support from GE Healthcare.

References

1. Williams DS, Detre JA, Leigh JS, Koretsky AP. Magnetic resonance imaging of perfusion using spin inversion of arterial water. Proc Natl Acad Sci U S A. 1992; 89(1):212–216. [PubMed: 1729691]
2. Kwong KK, Belliveau JW, Chesler DA, et al. Dynamic magnetic resonance imaging of human brain activity during primary sensory stimulation. Proc Natl Acad Sci USA. 1992; 89:5675–5679. [PubMed: 1608978]
3. Detre JA, Leigh JS, Williams DS, Koretsky AP. Perfusion imaging. Magn Reson Med. 1992; 23(1): 37–45. [PubMed: 1734182]
4. Edelman RR, Siewert B, Darby DG, et al. Qualitative mapping of cerebral blood flow and functional localization with echo-planar MR imaging and signal targeting with alternating radio frequency. Radiology. 1994; 192(2):513–520. [PubMed: 8029425]
5. Kim SG. Quantification of relative cerebral blood flow change by flow-sensitive alternating inversion recovery (FAIR) technique: application to functional mapping. Magn Reson Med. 1995; 34(3):293–301. [PubMed: 7500865]
6. Wong EC, Buxton RB, Frank LR. Implementation of quantitative perfusion imaging techniques for functional brain mapping using pulsed arterial spin labeling. NMR Biomed. 1997; 10(4–5):237–249. [PubMed: 9430354]
7. Golay X, Stuber M, Pruessmann KP, Meier D, Boesiger P. Transfer insensitive labeling technique (TILT): application to multislice functional perfusion imaging. J Magn Reson Imaging. 1999; 9(3): 454–461. [PubMed: 10194717]
8. Dai WY, Garcia D, de Bazelaire C, Alsop DC. Continuous Flow-Driven Inversion for Arterial Spin Labeling Using Pulsed Radio Frequency and Gradient Fields. Magn Reson Med. 2008; 60(6):1488–1497. [PubMed: 19025913]
9. Brown GG, Clark C, Liu TT. Measurement of cerebral perfusion with arterial spin labeling: Part 2. Applications. J Int Neuropsychol Soc. 2007; 13(3):526–538. [PubMed: 17445302]
10. Detre JA, Rao H, Wang DJ, Chen YF, Wang Z. Applications of arterial spin labeled MRI in the brain. J Magn Reson Imaging. 2012; 35(5):1026–1037. [PubMed: 22246782]

Author Manuscript Author Manuscript Author Manuscript Author Manuscript

11. Hendrikse J, Petersen ET, Golay X. Vascular disorders: insights from arterial spin labeling. Neuroimaging Clin N Am. 2012; 22(2):259–269. x–xi. [PubMed: 22548931]
12. Bokkers RP, van der Worp HB, Mali WP, Hendrikse J. Noninvasive MR imaging of cerebral perfusion in patients with a carotid artery stenosis. Neurology. 2009; 73(11):869–875. [PubMed: 19752454]
13. Macintosh BJ, Marquardt L, Schulz UG, Jezzard P, Rothwell PM. Hemodynamic alterations in vertebrobasilar large artery disease assessed by arterial spin-labeling MR imaging. AJNR Am J Neuroradiol. 2012; 33(10):1939–1944. [PubMed: 22555580]
14. Gonzalez-At JB, Alsop DC, Detre JA. Cerebral perfusion and arterial transit time changes during task activation determined with continuous arterial spin labeling. Magn Reson Med. 2000; 43(5): 739–746. [PubMed: 10800040]
15. Gunther M, Bock M, Schad LR. Arterial spin labeling in combination with a look-locker sampling strategy: inflow turbo-sampling EPI-FAIR (ITS-FAIR). Magn Reson Med. 2001; 46(5):974–984. [PubMed: 11675650]
16. Buxton RB, Frank LR, Wong EC, Siewert B, Warach S, Edelman RR. A general kinetic model for quantitative perfusion imaging with arterial spin labeling. Magn Reson Med. 1998; 40:383–396. [PubMed: 9727941]
17. Wang DJ, Alsop DC, Song HK, et al. Arterial transit time imaging with flow encoding arterial spin tagging (FEAST). Magn Reson Med. 2003; 50(3):599–607. [PubMed: 12939768]
18. Alsop DC, Detre JA, Golay X, et al. Recommended implementation of arterial spin-labeled perfusion MRI for clinical applications: A consensus of the ISMRM perfusion study group and the European consortium for ASL in dementia. Magn Reson Med. 2015; 73(1):102–116. [PubMed: 24715426]
19. Gunther M. Highly efficient accelerated acquisition of perfusion inflow series by cycled arterial spin labeling. Proceedings of the 15th Annual Meeting of ISMRM, Berlin, Germany. 2007 (abstract 380).
20. Wells JA, Lythgoe MF, Gadian DG, Ordidge RJ, Thomas DL. In vivo Hadamard encoded continuous arterial spin labeling (H-CASL). Magn Reson Med. 2010; 63(4):1111–1118. [PubMed: 20373414]
21. Dai W, Shankaranarayanan A, Alsop DC. Volumetric measurement of perfusion and arterial transit delay using hadamard encoded continuous arterial spin labeling. Magn Reson Med. 2013; 69(4): 1014–1022. [PubMed: 22618894]
22. Johnston ME, Lu K, Maldjian JA, Jung Y. Multi-TI Arterial Spin Labeling MRI with Variable TR and Bolus Duration for Cerebral Blood Flow and Arterial Transit Time Mapping. IEEE Trans Med Imaging. 2015; 34(6):1392–1402. [PubMed: 25616010]
23. Alsop DC, Detre JA. Reduced transit-time sensitivity in noninvasive magnetic resonance imaging of human cerebral blood flow. J Cereb Blood Flow Metab. 1996; 16(6):1236–1249. [PubMed: 8898697]
24. Lu H, Clingman C, Golay X, van Zijl PC. Determining the longitudinal relaxation time (T1) of blood at 3.0 Tesla. Magn Reson Med. 2004; 52(3):679–682. [PubMed: 15334591]
25. Dai WY, Robson PM, Shankaranarayanan A, Alsop DC. Sensitivity Calibration With a Uniform Magnetization Image to Improve Arterial Spin Labeling Perfusion Quantification. Magn Reson Med. 2011; 66(6):1590–1600. [PubMed: 21523824]
26. Dai WY, Robson PM, Shankaranarayanan A, Alsop DC. Reduced resolution transit delay prescan for quantitative continuous arterial spin labeling perfusion imaging. Magn Reson Med. 2012; 67(5):1252–1265. [PubMed: 22084006]
27. Ye FQ, Mattay VS, Jezzard P, Frank JA, Weinberger DR, McLaughlin AC. Correction for vascular artifacts in cerebral blood flow values measured by using arterial spin tagging techniques. Magn Reson Med. 1997; 37(2):226–235. [PubMed: 9001147]
28. Schepers J, van Osch MJP, Nicolay K. Effect of vascular crushing on FAIR perfusion kinetics, using a BIR-4 pulse in a magnetization prepared FLASH sequence. Magn Reson Med. 2003; 50(3):608–613. [PubMed: 12939769]
29. Herscovitch P, Raichle ME. What is the correct value for the brain-blood partition coefficient for water? J Cereb Blood Flow Metab. 1985; 5:65–69. [PubMed: 3871783]

Author Manuscript Author Manuscript Author Manuscript Author Manuscript

30. Garcia DM, Duhamel G, Alsop DC. Efficiency of inversion pulses for background suppressed arterial spin labeling. Magn Reson Med. 2005; 54(2):366–372. [PubMed: 16032674]
31. Mazziotta J, Toga A, Evans A, et al. A probabilistic atlas and reference system for the human brain: International Consortium for Brain Mapping (ICBM). Philos Trans R Soc Lond B Biol Sci. 2001; 356(1412):1293–1322. [PubMed: 11545704]
32. Jenkinson M, Beckmann CF, Behrens TE, Woolrich MW, Smith SM. Fsl. Neuroimage. 2012; 62(2):782–790. [PubMed: 21979382]
33. Satopaa V, Albrecht J, Irwin D, Raghavan B. Finding a 'Kneedle' in a Haystack: Detecting Knee Points in System Behavior. IEEE ICDCS SIMPLEX Workshop. 2011
34. Cavusoglu M, Pohmann R, Burger HC, Uludag K. Regional effects of magnetization dispersion on quantitative perfusion imaging for pulsed and continuous arterial spin labeling. Magn Reson Med. 2013; 69(2):524–530. [PubMed: 22488815]
35. Chappell MA, Woolrich MW, Kazan S, Jezzard P, Payne SJ, MacIntosh BJ. Modeling dispersion in arterial spin labeling: Validation using dynamic angiographic measurements. Magn Reson Med. 2013; 69(2):563–570. [PubMed: 22489046]
36. Chappell MA, MacIntosh BJ, Donahue MJ, Gunther M, Jezzard P, Woolrich MW. Separation of Macrovascular Signal in Multi-inversion Time Arterial Spin Labelling MRI. Magn Reson Med. 2010; 63(5):1357–1365. [PubMed: 20432306]
37. White N, Roddey C, Shankaranarayanan A, et al. PROMO: Real-Time Prospective Motion Correction in MRI Using Image-Based Tracking. Magn Reson Med. 2010; 63(1):91–105. [PubMed: 20027635]
38. Zun Z, Shankaranarayanan A, Zaharchuk G. Pseudocontinuous arterial spin labeling with prospective motion correction (PCASL-PROMO). Magn Reson Med. 2014; 72(4):1049–1056. [PubMed: 24243585]
39. von Samson-Himmelstjerna F, Madai VI, Sobesky J, Guenther M. Walsh-ordered hadamard time-encoded pseudocontinuous ASL (WH pCASL). Magn Reson Med. 2016; 76(6):1814–1824. [PubMed: 26714671]
40. Mezue M, Segerdahl AR, Okell TW, Chappell MA, Kelly ME, Tracey I. Optimization and reliability of multiple postlabeling delay pseudo-continuous arterial spin labeling during rest and stimulus-induced functional task activation. J Cereb Blood Flow Metab. 2014; 34(12):1919–1927. [PubMed: 25269517]

Author Manuscript Author Manuscript Author Manuscript Author Manuscript

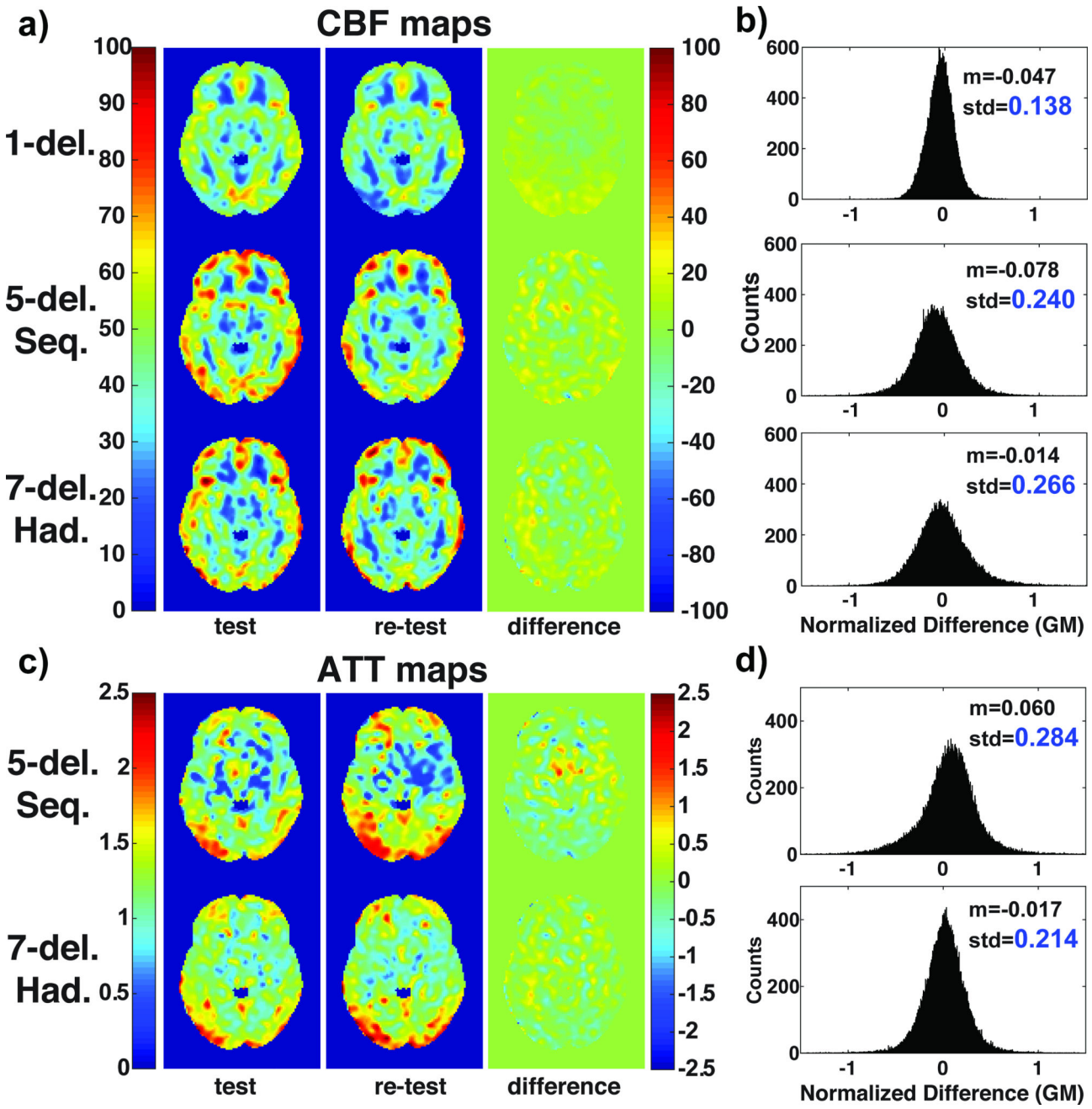

Figure 1.

Examples of cerebral blood flow (CBF, a, unit ml/100 g/min) and arterial transit time (ATT, c, unit s) maps acquired in test and retest scans and their difference in a representative subject. (b) and (d) are the histograms of the corresponding difference maps, with the voxels counts from the gray matter of the whole brain. The standard deviations of the difference shown in blue in (b) and (d) were used as the measure of the reproducibility.

Author Manuscript Author Manuscript Author Manuscript Author Manuscript

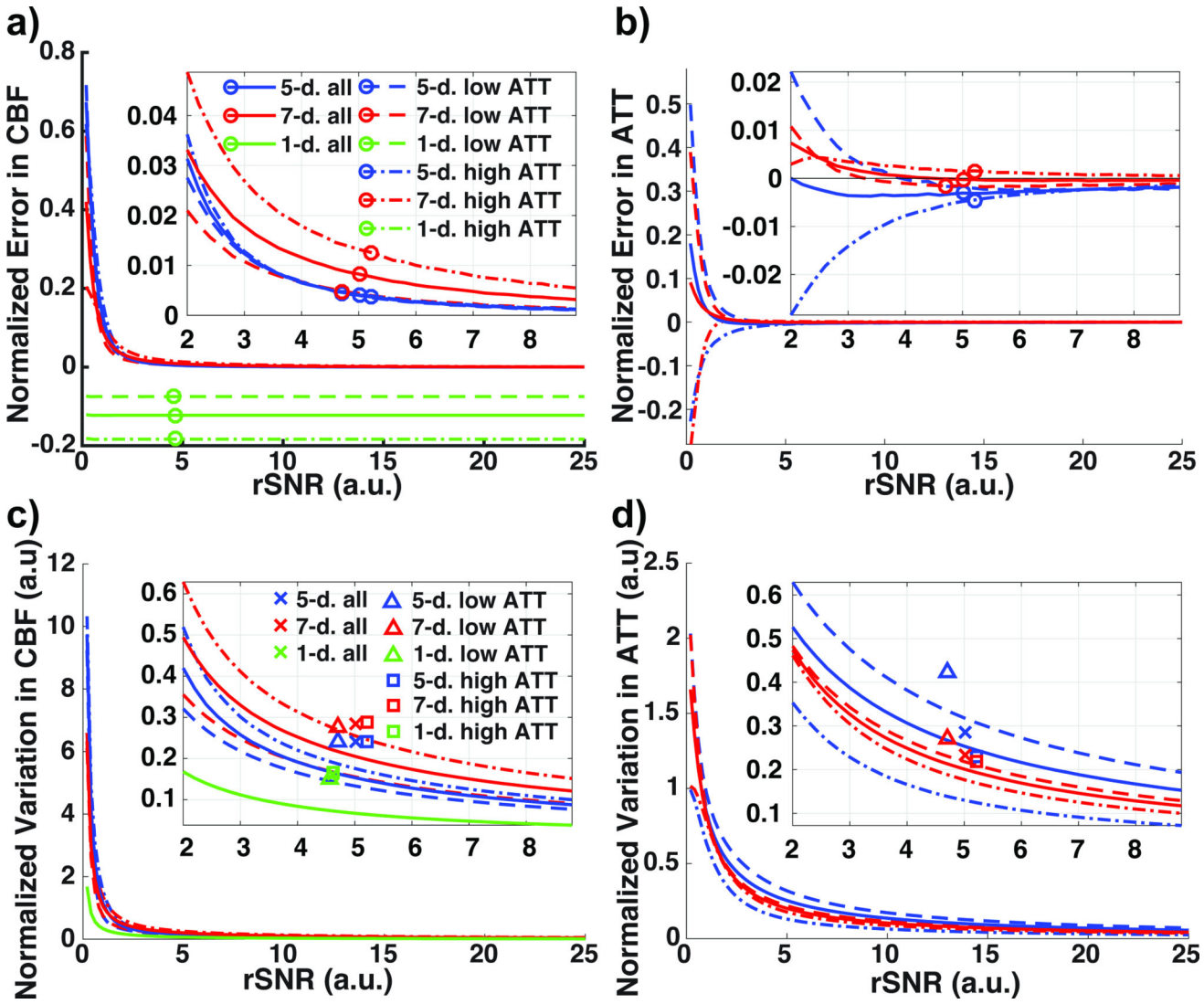

Figure 2.

Mean normalized errors (a and b) and variations (c and d) between repeated measurements of cerebral blood flow (CBF) and arterial transit time (ATT) at different relative signl-to-noise ratio (rSNR) levels and in different ATT ranges (low: dashed lines; high: dotted dashed lines and all: solid lines) from the simulations. The colored circles in a and b on the curves indicate the predicted normalized errors at the measured rSNR levels from the in vivo experiments with vascular crushing. The colored symbols in c and d indicate the measured normalized variations at the measured rSNR levels in different ATT ranges (low: triangle; high: square and all: cross), showing good agreement with the simulation predictions.

Author Manuscript Author Manuscript Author Manuscript Author Manuscript

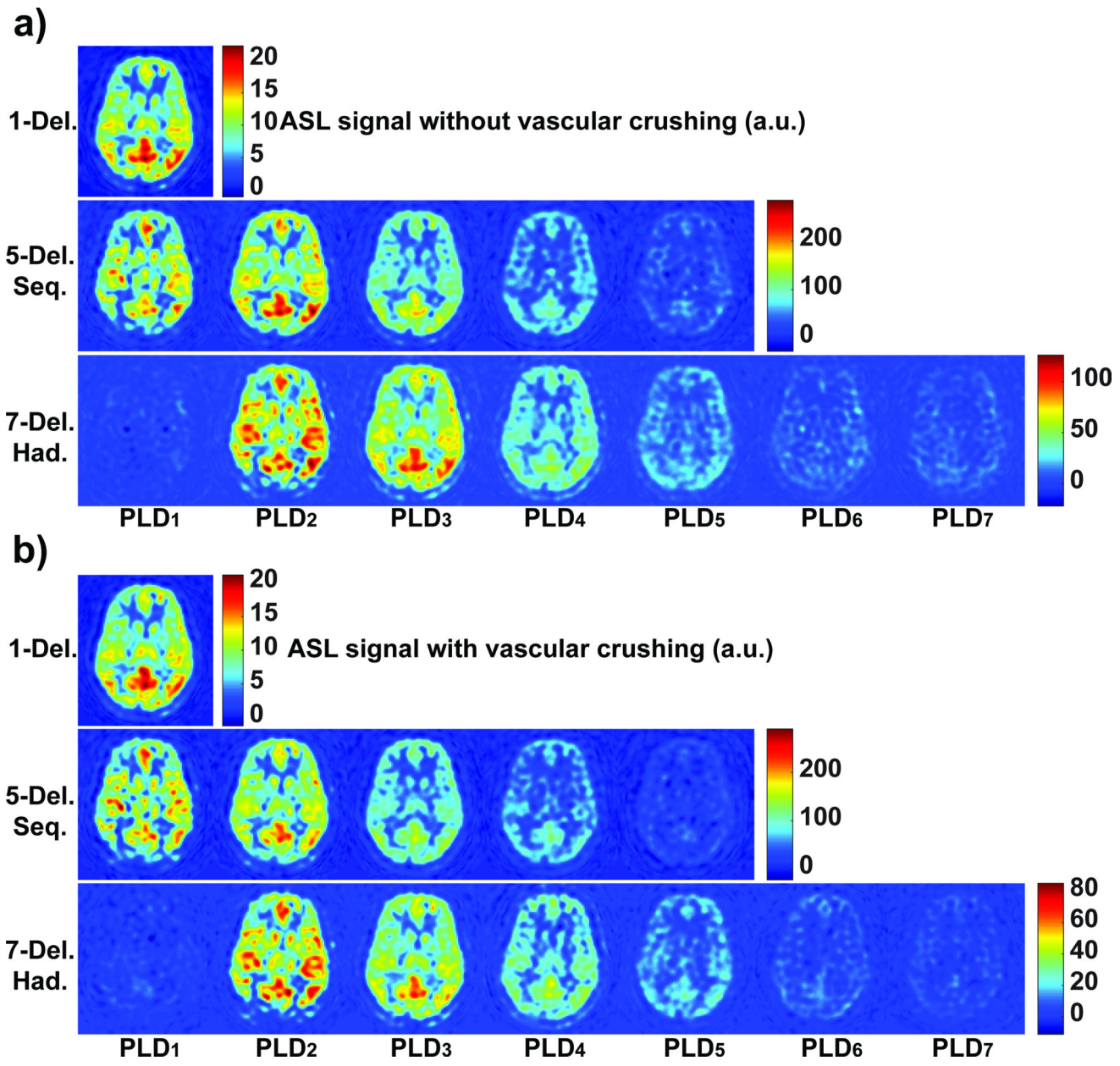

Figure 3.

Representative raw arterial spin labeling (ASL) signals (arbitrary unit) in one slice, measured at different post-labeling delays (PLDs) with 1-del., 5-del. Seq. and 7-del. Had., without (a) and with (b) vascular crushing. The color scales were adjusted so noise levels in different scans can be visually appreciated.

Author Manuscript Author Manuscript Author Manuscript Author Manuscript

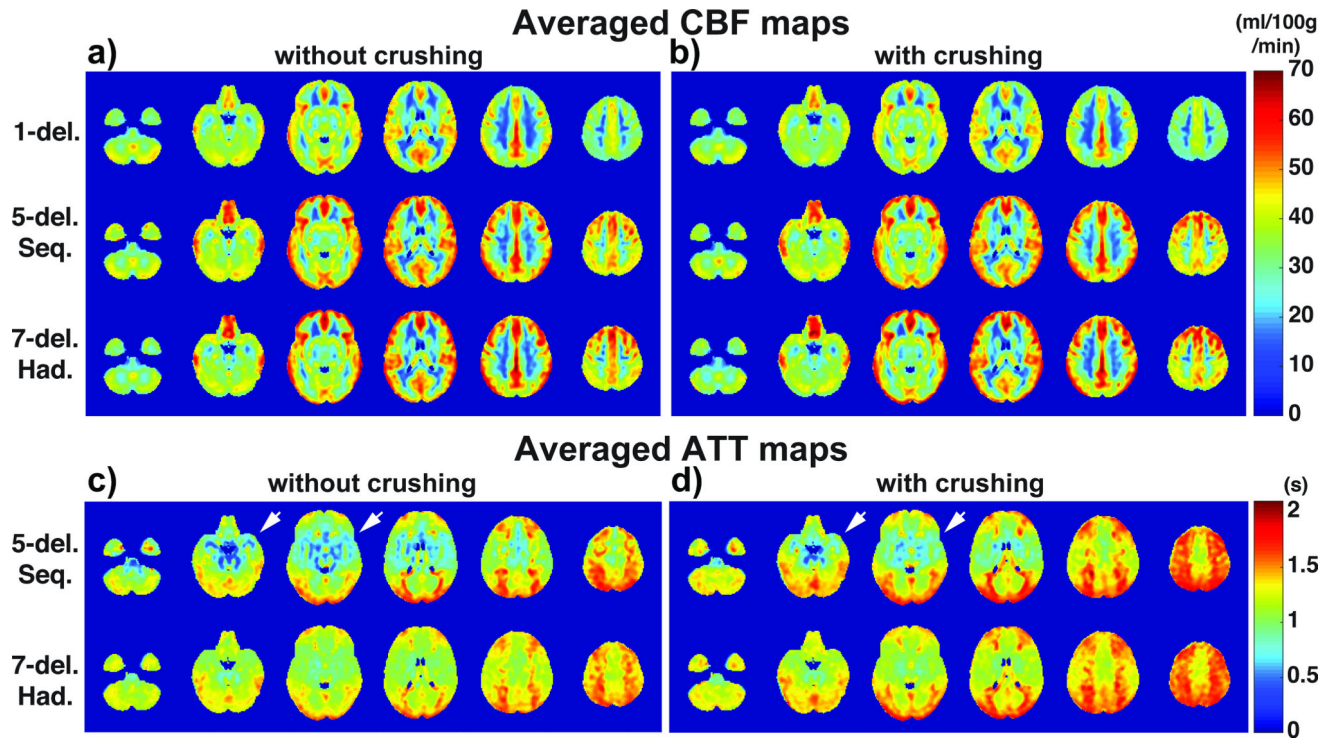

Figure 4.

The averaged cerebral blood flow (CBF, without and with vascular crushing, a and b, respectively) and arterial transit time (ATT, without and with vascular crushing, c and d, respectively) maps across the subjects, shown in a common MNI space. 1-del. labeling showed lower CBF, especially in regions detected with long ATT; while the other two multi-delay methods yielded comparable CBF maps. 5-del. Seq. labeling showed stronger intravascular effects in ATT maps (in voxels large arteries reside, indicated by white arrows) compared to 7-del. Had. labeling, both without and with vascular crushing.

Author Manuscript Author Manuscript Author Manuscript Author Manuscript

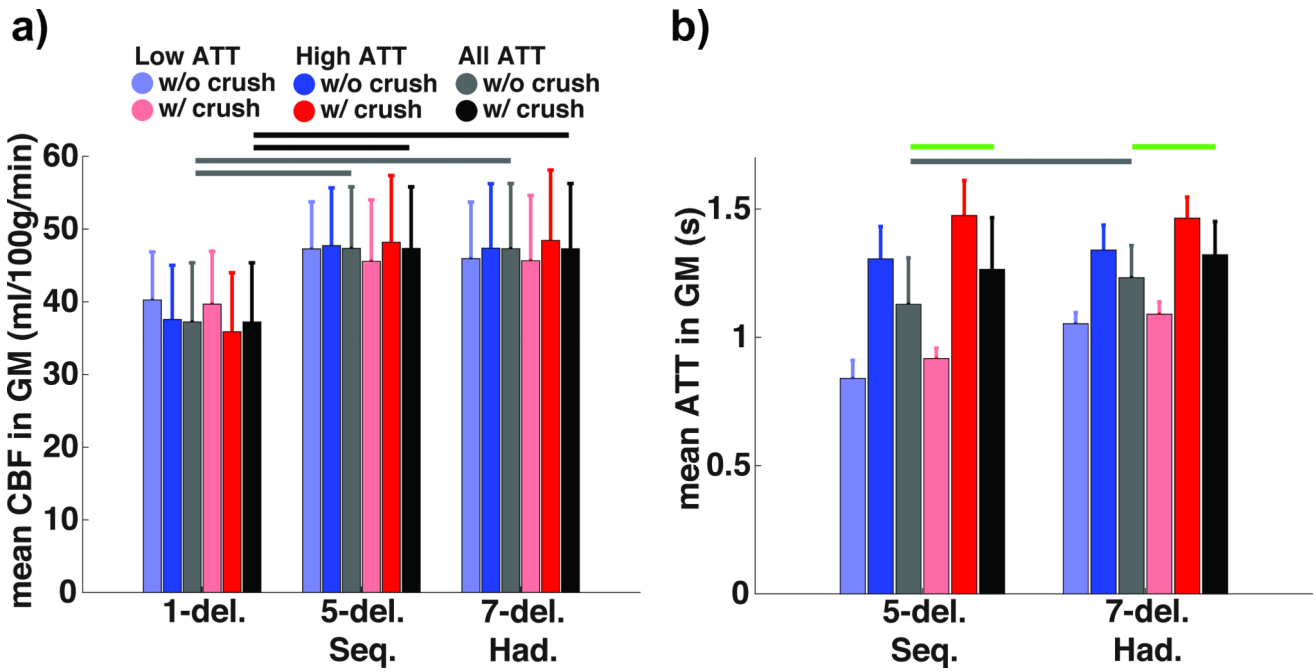

Figure 5.

Averaged cerebral blood flow (CBF, a) and arterial transit time (ATT, b) measured without (blue and gray) and with (red and black) vascular crushing, in gray matter (GM) with low ATT (light color), high ATT (full color) and all ATT (colorless), from the in vivo study. The error bars show the standard errors of the means. Significant differences found between two measurement conditions are indicated by the horizontal bars at the top, where comparisons without and with crushing are shown in gray and black, respectively; and comparisons between crushing conditions in green. For brevity, only the comparison in all ATT regions of interest (ROIs) are shown; for comparisons in low and high ATT ROIs, please refer to the *P*-values listed in Tables 2 and 3. 5-del. Seq. and 7-del. Had. gave comparable CBF in GM; while 1-del. underestimated CBF. ATTs measured with vascular crushing were longer than those without crushing, indicating the additional time needed for blood to reach the microvasculature in imaging voxels.

Author Manuscript Author Manuscript Author Manuscript Author Manuscript

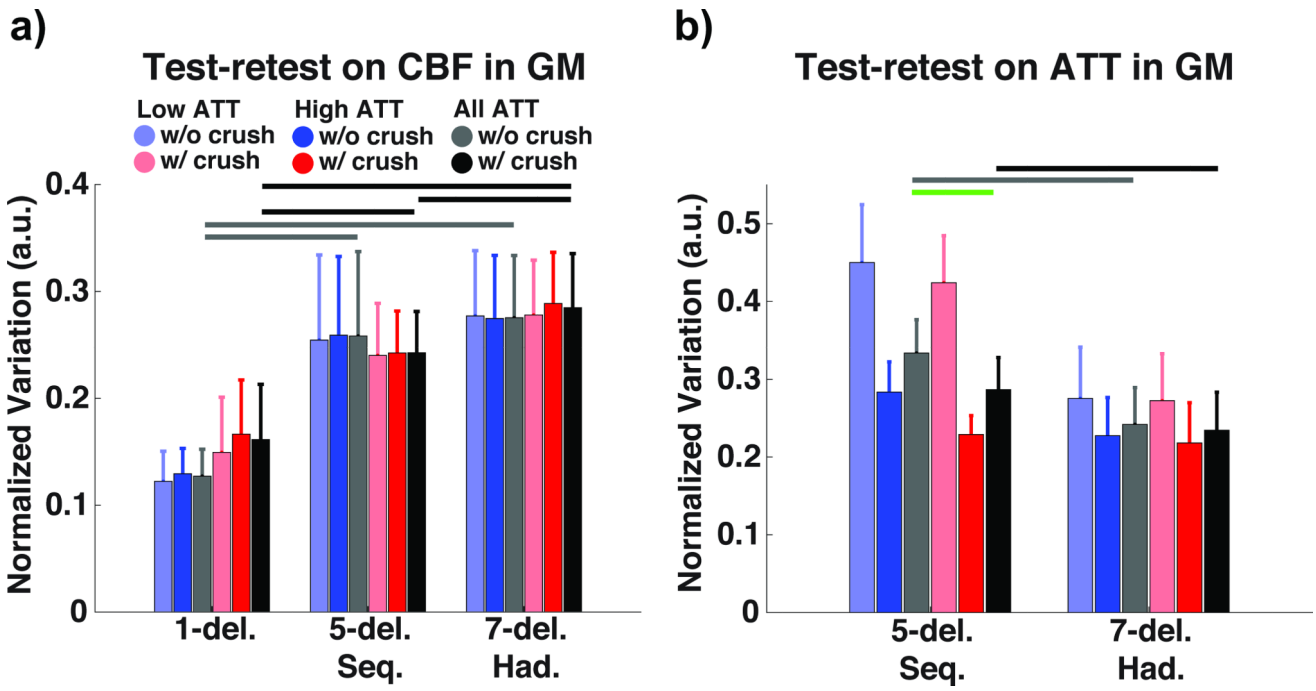

Figure 6.

Normalized variations between repeated measurements of cerebral blood flow (CBF, a) and arterial transit time (ATT, b), without (blue and gray) and with (red and black) vascular crushing, in gray matter (GM) with low ATT (light color), high ATT (full color) and all ATT (colorless), averaged across subjects. Significant differences found between two measurement conditions are indicated by the horizontal bars at the top, where comparisons without and with crushing are shown in gray and black, respectively; and comparisons between crushing conditions in green. For brevity, only the comparison in all ATT regions of interest (ROIs) are shown; for comparisons in low and high ATT ROIs, please refer to the *P*-values listed in Tables 2 and 3). 1-del. showed the lowest variation in CBF estimation; while 5-del. Seq. (except with crushing) and 7-del. Had. gave comparable variations. 7-del. Had. was more reproducible than 5-del. Seq. in ATT measurements.

Author Manuscript Author Manuscript Author Manuscript Author Manuscript

J Magn Reson Imaging. Author manuscript; available in PMC 2019 April 01.

Table 1

Mean cerebral blood flow (CBF) and arterial transit time (ATT) estimates in gray matter (GM) regions of interest (ROIs) with different ATT ranges, and the corresponding normalized variations, averaged across subjects (n = 10, mean ± standard deviation).

Labeling	GM ROI	W/O Crushing	W/ Crushing	W/O Crushing	W/ Crushing
		CBF			
		Average CBF in GM (ml/100 g/min)		Average normalized variation of CBF in GM (a.u.)	
1-del.	Low ATT	40.3 ± 6.6	39.7 ± 7.2	0.122 ± 0.028	0.149 ± 0.052
	High ATT	37.6 ± 7.5	35.9 ± 8.1	0.129 ± 0.024	0.166 ± 0.051
	All	38.4 ± 7.4	37.2 ± 8.1	0.127 ± 0.025	0.161 ± 0.052
5-del. Seq.	Low ATT	47.3 ± 6.5	45.6 ± 8.5	0.254 ± 0.080	0.240 ± 0.049
	High ATT	47.7 ± 8.0	48.2 ± 9.2	0.258 ± 0.074	0.242 ± 0.039
	All	47.5 ± 7.1	47.3 ± 8.5	0.258 ± 0.079	0.242 ± 0.039
7-del. Had.	Low ATT	45.9 ± 7.8	45.7 ± 9.0	0.276 ± 0.061	0.277 ± 0.051
	High ATT	47.4 ± 8.9	48.4 ± 9.7	0.274 ± 0.059	0.288 ± 0.048
	All	46.8 ± 8.1	47.3 ± 9.0	0.275 ± 0.058	0.284 ± 0.051
		ATT			
		Average ATT in GM (s)		Average normalized variation of ATT in GM (a.u.)	
5-del. Seq.	Low ATT	0.84 ± 0.071	0.92 ± 0.041	0.450 ± 0.075	0.424 ± 0.061
	High ATT	1.31 ± 0.13	1.48 ± 0.14	0.283 ± 0.039	0.228 ± 0.024
	All	1.13 ± 0.18	1.27 ± 0.20	0.333 ± 0.043	0.286 ± 0.041
7-del. Had.	Low ATT	1.05 ± 0.044	1.09 ± 0.049	0.275 ± 0.066	0.272 ± 0.060
	High ATT	1.34 ± 0.097	1.47 ± 0.082	0.227 ± 0.049	0.218 ± 0.052
	All	1.23 ± 0.13	1.32 ± 0.13	0.241 ± 0.048	0.234 ± 0.049

W/O = without, W/ = with, a.u. = arbitrary unit.

Author Manuscript Author Manuscript Author Manuscript Author Manuscript

Table 2

P-values of the pairwise comparisons performed on cerebral blood flow (CBF) and arterial transit time (ATT) between sequences in gray matter (GM) regions of interest (ROIs) with different ATT ranges and under different vascular crushing conditions.

	Comparison on mean estimates						Comparison on normalized variation between repeated runs					
	Without crushing			With crushing			Without crushing			With crushing		
	Low ATT	High ATT	All	Low ATT	High ATT	All	Low ATT	High ATT	All	Low ATT	High ATT	All
CBF												
1d vs. 5d	$^{*}5.2 \times 10^{-7}$	$^{*}2.5 \times 10^{-8}$	$^{*}2.0 \times 10^{-8}$	$^{*}7.2 \times 10^{-6}$	$^{*}7.2 \times 10^{-7}$	$^{*}1.8 \times 10^{-6}$	$^{*}3.7 \times 10^{-5}$	$^{*}4.1 \times 10^{-5}$	$^{*}5.5 \times 10^{-5}$	$^{*}8.5 \times 10^{-4}$	$^{*}3.6 \times 10^{-3}$	$^{*}9.7 \times 10^{-4}$
1d vs. 7d	$^{*}1.1 \times 10^{-4}$	$^{*}4.5 \times 10^{-6}$	$^{*}6.5 \times 10^{-6}$	$^{*}1.3 \times 10^{-4}$	$^{*}3.0 \times 10^{-7}$	$^{*}2.7 \times 10^{-6}$	$^{*}5.3 \times 10^{-6}$	$^{*}8.1 \times 10^{-6}$	$^{*}4.7 \times 10^{-6}$	$^{*}1.6 \times 10^{-4}$	$^{*}5.3 \times 10^{-5}$	$^{*}7.1 \times 10^{-5}$
5d vs. 7d	0.19	0.72	0.49	0.91	0.71	0.95	0.18	0.28	0.29	$^{*}7.7 \times 10^{-4}$	$^{*}5.7 \times 10^{-4}$	$^{*}4.7 \times 10^{-4}$
1d (L vs. H)		$^{*}2.7 \times 10^{-3}$			$^{*}8.2 \times 10^{-5}$			0.062			$^{*}0.015$	
5d (L vs. H)		0.60			$^{*}9.9 \times 10^{-3}$			0.65			0.82	
7d (L vs. H)		0.12			$^{*}5.6 \times 10^{-3}$			0.75			0.13	
ATT												
5dvs. 7d	$^{*}3.9 \times 10^{-6}$	$^{*}1.0 \times 10^{-4}$	$^{*}2.3 \times 10^{-3}$	0.12	0.72	0.12	$^{*}2.5 \times 10^{-7}$	$^{*}2.1 \times 10^{-6}$	$^{*}9.0 \times 10^{-5}$	$^{*}3.3 \times 10^{-4}$	0.52	$^{*}0.033$
5d (L vs. H)		$^{*}1.6 \times 10^{-7}$			$^{*}8.1 \times 10^{-8}$			$^{*}6.3 \times 10^{-7}$			$^{*}1.9 \times 10^{-6}$	
7d (L vs. H)		$^{*}1.4 \times 10^{-6}$			$^{*}7.2 \times 10^{-8}$			$^{*}8.6 \times 10^{-4}$			$^{*}3.6 \times 10^{-4}$	

Those passing the Bonferroni-corrected significance threshold are labeled with asterisks.

Author Manuscript Author Manuscript Author Manuscript Author Manuscript

Table 3

P-values of the comparisons performed on cerebral blood flow (CBF) and arterial transit time (ATT) in gray matter (GM) regions of interest (ROIs) with different ATT ranges measured with and without vascular crushing.

		CBF			ATT	
		1-del.	**5-del. Seq.**	**7-del. Had.**	**5-del. Seq.**	**7-del. Had.**
Mean estimates	Low ATT	0.42	*0.031	0.74	*0.018	*4.3×10^{-3}
	High ATT	0.078	0.57	0.23	*1.9×10^{-4}	*6.9×10^{-5}
	All	0.16	0.81	0.56	*6.7×10^{-4}	*9.0×10^{-5}
Normalized variations	Low ATT	0.17	0.42	0.94	0.26	0.79
	High ATT	0.062	0.32	0.31	*1.3×10^{-3}	0.45
	All	0.076	0.38	0.45	*8.1×10^{-3}	0.53

Those passing the Bonferroni-corrected significance threshold are labeled with asterisks.

Author Manuscript Author Manuscript Author Manuscript Author Manuscript

Table 4

Mean signal-to-noise ratio (SNR, arbitrary unit, a.u., mean ± standard deviation) of arterial spin labeling (ASL) signals measured in gray matter (GM) regions of interest (ROIs) with different arterial transit time (ATT) ranges, at different post-labeling delays (PLDs), and the calculated relative SNR (rSNR, a.u.) at one PLD (PLD_1 in 1-del., PLD_3 in 5-del. Seq. and 7-del. Had. rSNRs for 7-del. Had. were duplicated from 5-del. Seq., see text).

		PLD_1	PLD_2	PLD_3	PLD_4	PLD_5	PLD_6	PLD_7	rSNR
SNR without crushing									
1-del.	Low ATT	9.19 ± 1.82							4.94 ± 0.98
	High ATT	9.73 ± 2.05							5.09 ± 1.07
	All	9.55 ± 1.96							5.05 ± 1.04
5-del. Seq.	Low ATT	13.58 ± 3.69	13.90 ± 4.44	9.37 ± 2.74	5.72 ± 1.56	3.27 ± 0.92			4.93 ± 1.44
	High ATT	10.68 ± 2.93	13.24 ± 4.31	10.67 ± 3.27	6.78 ± 1.67	3.94 ± 1.07			5.46 ± 1.67
	All	11.88 ± 3.65	13.54 ± 4.46	10.16 ± 2.89	6.39 ± 1.47	3.69 ± 0.91			5.25 ± 1.50
7-del. Had.	Low ATT	0.33 ± 0.42	12.61 ± 4.26	10.64 ± 3.44	5.85 ± 2.20	4.22 ± 0.97	1.98 ± 0.60	1.41 ± 0.65	4.93 ± 1.44
	High ATT	0.25 ± 0.44	8.95 ± 3.32	11.25 ± 3.58	7.21 ± 2.63	5.09 ± 1.04	2.45 ± 0.74	1.73 ± 0.68	5.46 ± 1.67
	All	0.28 ± 0.43	10.49 ± 4.26	11.00 ± 3.45	6.67 ± 2.27	4.75 ± 0.91	2.26 ± 0.61	1.60 ± 0.62	5.25 ± 1.50
SNR with crushing									
1-del.	Low ATT	8.49 ± 2.16							4.57 ± 1.16
	High ATT	8.85 ± 2.16							4.63 ± 1.13
	All	8.73 ± 2.12							4.61 ± 1.12
5-del. Seq.	Low ATT	12.52 ± 3.87	12.93 ± 3.92	8.97 ± 2.23	4.99 ± 1.54	3.02 ± 0.78			4.72 ± 1.17
	High ATT	9.63 ± 3.28	11.98 ± 3.58	10.18 ± 2.37	6.00 ± 1.67	3.66 ± 0.68			5.21 ± 1.21
	All	10.83 ± 3.98	12.41 ± 3.88	9.72 ± 2.13	5.61 ± 1.47	3.43 ± 0.62			5.02 ± 1.10
7-del. Had.	Low ATT	0.68 ± 0.53	11.22 ± 3.80	9.91 ± 2.68	5.34 ± 1.30	4.05 ± 1.11	1.82 ± 0.66	1.13 ± 0.39	4.72 ± 1.17
	High ATT	0.35 ± 0.38	7.27 ± 2.64	10.02 ± 2.78	6.60 ± 1.34	4.94 ± 1.17	2.72 ± 0.70	1.98 ± 0.32	5.21 ± 1.21
	All	0.48 ± 0.48	8.90 ± 3.73	9.97 ± 2.71	6.12 ± 1.22	4.64 ± 1.06	2.38 ± 0.56	1.66 ± 0.28	5.02 ± 1.10